1 **Underestimation of Column NO$_2$ Amounts from the OMI Satellite Compared to Diurnally**

2 **Varying Ground-Based Retrievals from Multiple Pandora Spectrometer Instruments**

3 Jay Herman[1], Nader Abuhassan[1], Jhoon Kim[2], Jae Kim[3], Manvendra Dubey[4], Marcelo Raponi[5],

4 Maria Tzortziou[6]

5 **Abstract**

6 Retrievals of Total Column NO$_2$ (TCNO$_2$) are compared for 14 sites from the Ozone Measuring

7 Instrument (OMI using OMNO2-NASA v3.1) on the AURA satellite and from multiple ground-

8 based PANDORA spectrometer instruments making direct-sun measurements. While OMI

9 accurately provides the daily global distribution of retrieved TCNO$_2$, OMI almost always

10 underestimates the local amount TCNO$_2$ by 50 to 100% in polluted areas, while occasionally the

11 daily OMI value exceeds that measured by PANDORA at very clean sites. Compared to local

12 ground-based or aircraft measurements, OMI cannot resolve spatially variable TCNO$_2$ pollution

13 within a city or urban areas, which makes it less suitable for air quality assessments related to

14 human health. In addition to systematic underestimates in polluted areas, OMI's selected 13:30

15 equator crossing time polar orbit causes it to miss the frequently much higher values of TCNO$_2$

16 that occur before or after the OMI overpass time. Six discussed Northern Hemisphere PANDORA

17 sites have multi-year data records (Busan, Seoul, Washington DC, Waterflow New Mexico,

18 Boulder Colorado, and Mauna Loa) and one site in the Southern Hemisphere (Buenos Aires

19 Argentina). The first four of these sites and Buenos Aires frequently have high TCNO$_2$ (TCNO$_2$ >

20 0.5 DU). Eight additional sites have shorter term data records in the US and South Korea. One of

21 these is a one-year data record from a highly polluted site at City College in New York City with

22 pollution levels comparable to Seoul, South Korea. OMI estimated air mass factor, surface

23 reflectivity, and the OMI 24x13 km^2 FOV (field of view) are three factors that can cause OMI to

24 underestimate TCNO$_2$. Because of the local inhomogeneity of NO$_x$ emissions, the large OMI FOV

25 is the most likely factor for consistent underestimates when comparing OMI TCNO$_2$ to retrievals

26 from the small PANDORA effective FOV (measured in m^2) calculated from the solar diameter of

27 0.5^O.

29 **Key Words: Nitrogen dioxide, OMI, PAN, PANDORA, ground-based, satellite**

Correspondence email: jay.r.herman@nasa.gov

[1]University of Maryland Baltimore County JCET, Maryland
[2]Department of Atmospheric Sciences, Yonsei National University, South Korea
[3]Department of Atmospheric Science, Pusan National University, South Korea
[4]Earth Systems Observations, Los Alamos National Laboratory, Los Alamos, NM 87545
[5]Departamento de Investigaciones en Láseres y Aplicaciones (DEILAP), Instituto de Investigaciones
Científicas y Técnicas para la Defensa (CITEDEF), Ministerio de Defensa (MINDEF), Buenos Aires, Argentina
[6]City College of New York, New York City, NY

Underestimation of Column NO$_2$ Amounts from the OMI Satellite Compared to Ground-Based Retrievals from Multiple Pandora Spectrometer Instruments

1.0 Introduction

Retrieval of Total Column NO$_2$ (TCNO$_2$) from the Ozone Monitoring Instrument (OMI) has been a scientific success story for the past 14 years. Near total global coverage from the well-calibrated OMI has enabled observation of all the regions where NO$_2$ is produced and has permitted monitoring of the changes during the 2004 to 2019 period, especially in regions where there is heavy and growing industrial activity (e.g., China and India). TCNO$_2$ amounts (data used: OMNO2-NASA v3.1) retrieved from OMI over various specified land locations show a strong local underestimate compared to co-located PANDORA Spectrometer Instruments (the abbreviation PAN is used for graph and table labels). The underestimate of OMI TCNO$_2$ at the overpass time compared to ground-based measurements has previously been reported at a few specific locations (Bechle, 2013; Lamsal et al., 2015; Ialongo et al., 2017; Kollonige, et al., 2018; Goldberg et al., 2018; Herman et al., 2018). The accuracy and precision of PANDORA TCNO$_2$ measurements has been previously discussed (Herman et al., 2009; 2018). For any location, the OMI overpass local standard time consists of the central overpass near the 13:30 hour equator crossing solar time and occasionally a side viewing overpass from adjacent orbits within ±90 minutes of the central overpass time. Independently from instrument calibration and retrieval errors, there are two specific aspects to the underestimation of TCNO$_2$ pollution levels. Because of OMI's selected polar orbit, it is not possible for the mid-day OMI observations to see the large diurnal variation of TCNO$_2$ that usually occur after the 13:30 overpass time, and second, because of spatial inhomogeneity the large OMI field of view (FOV) footprint 13 x 24 km^2 at OMI nadir view tends to average regions of high NO$_2$ amounts (Nowlan et al., 2016; Judd et al., 2018) with those from lower pollution areas. An analysis by Judd et al., (2019, their Fig. 9) shows the effect of decreasing satellite spatial resolution on improving agreement with PANDORA, with the best agreement occurring with an airborne instrument, GEO-TASO (resolution 3x3 km^2) followed by TropOMI (5x5 km^2) and then OMI (18x18 km^2). Both OMI and TropOMI show an underestimate of TCNO$_2$ compared to PANDORA.

There are other possible systematic retrieval errors with OMI TCNO$_2$. The largest of these is determining the air mass factor (AMF) needed to convert slant column measurements into vertical column amounts followed by the surface reflectivity Rs (Boersma et al., 2011; Lin et al., 2015; Nowlan et al., 2016; Lorente et al., 2018). Accurately determining the AMF for TCNO$_2$ requires a-priori knowledge of the NO$_2$ profile shape (Krotkov et al., 2017), which is estimated from coarse resolution model calculations (Boersma et al., 2011), and using the correct Rs. Currently Rs is found using a statistical process of sorting through years of data to find relatively clear-sky scenes for each location (Kleipool, et al., 2008; O'Byrne et al., 2010). Boersma et al., 2004 gave a detailed error analysis for the various components contributing OMI TCNO$_2$ retrievals resulting an estimated "retrieval precision of 35-60%" in heavily polluted areas dominated by determining the air mass factor. An improved V2.0 DOMINO retrieval (Boersma et al., 2011) algorithm reduced the retrieval errors while increasing the estimated airmass factor, which reduces the retrieved TCNO$_2$ up to 20% in winter and 10% in summer. The current version of OMNO2-NASA (Krotkov et al., 2017) and v2.0 DOMINO (Boersma et al., 2011) are generally in good agreement (Marchenko et al.,

69   2015; Zara et al., 2018). However, the OMNO2-NASA $TCNO_2$ retrievals are 10 to 15% lower than the v2.0
70   DOMINO retrievals and with Quality Assurance for Essential Climate Variables (QA4ECV) retrievals. A
71   subsequent detailed analysis of surface reflectivity (Vasilkov et al., 2017) shows that retrieval of $TCNO_2$ in
72   highly polluted areas (e.g., some areas in China) can increase by 50% with the use of geometry-dependent
73   reflectivities, but only increase about 5% in less polluted areas. For PANDORA, calculation of the solar
74   viewing AMF is a simple geometric problem (AMF is approximately proportional to the cosecant of the
75   solar zenith angle SZA) and is independent of R_S (Herman et al., 2009). For a highly polluted region with
76    $TCNO_2$ = 5.34×10^{16} molecules/cm^2 or 2 DU, the PANDORA error is expected to be less than 2 ± 0.05 DU
77   (±2.5%) with the largest uncertainty coming from an assumed nominal amount of stratospheric $TCNO_2$ =
78   0.1 DU.

79   Accurate satellite $TCNO_2$ retrievals (and for other trace gases) are important in the estimate of
80   the effect of polluted air containing NO_2 on human health (Kim and Song, 2017 and references therein),
81   especially from the viewpoint of NO_2 as a respiratory irritant and precursor to cancer (Choudhari et al.,
82   2013). Since NO_2 is largely produced by combustion, satellite observations of NO_2 serve as a proxy for
83   changing industrial activity. Another important application requiring accurate measurements of the
84   amount of $TCNO_2$ and its diurnal variation is atmospheric NO_2 contribution to nitrification of coastal
85   waters (Tzortziou et al., 2018).

86   We show that the use of OMI $TCNO_2$ for estimating local air quality and coastal nitrification on a
87   global basis is misleading for most polluted locations, and especially on days when the morning or
88   afternoon amounts are higher than those occurring at the OMI overpass time near 13:30 hours standard
89   time. OMI $TCNO_2$ data are extremely useful for estimating regional pollution amounts and for assessing
90   long-term changes in these amounts. Modelling studies (Lamsal et al., 2017 Fig. 1) based on the Global
91   Modelling Initiative model (Strahan et al., 2007) simulating $TCNO_2$ diurnal variation over Maryland USA
92   (37-40°N, 74-79°W) shows a late afternoon peak and shows that the stratospheric component does not
93   substantially contribute to this peak. Boersma et al. (2016) show that sampling strategy can cause
94   systematic errors between OMI $TCNO_2$ and model $TCNO_2$ with satellite results being up to 20% lower than
95   models. Duncan et al., (2014) reviews the applicability of satellite $TCNO_2$ data to represent air quality and
96   notes that $TCNO_2$ correlates well with surface levels of NO_2 in industrial regions and states that the portion
97   of $TCNO_2$ in the boundary layer could be over 75% of the total vertical column depending on NO_2 altitude
98   profile shape.

99   This paper presents 14 different site comparisons between retrieved OMI $TCNO_2$ overpass values
100   that are co-located with PANDORA $TCNO_2$ amounts from various locations in the world. Six of the
101   comparisons are where PANDORAs have long-term data (1-year or longer) records. The comparisons are
102   done using 80 second cadence data matched to the OMI overpass times averaged over ±6 minutes and
103   with monthly running averages calculated using Lowess(f) (Locally Weighted least squares fit to a fraction
104   f of the data points, (Cleveland, 1981) of OMI-PANDORA time matched $TCNO_2$. OMI overpass data,
105   https://avdc.gsfc.nasa.gov/index.php?site=666843934&id=13, are filtered for the row anomaly and
106   cloudy pixels. The selection of a $\pm$6-minute window represents 720 seconds or 9 PANDORA
107   measurements averaged together around the OMI overpass time to reduce the effect of outlier points.
108   The specific value of ±6 minutes is arbitrary but increases the already high effective signal to noise ratio

109 by a factor of 3. PANDORA data are filtered for significant cloud cover by examining the effective variance
110 in sub-interval (20 seconds) measurements. Each PANDORA listed measurement is the average of up to
111 4000 (clear sky) individual measurement made over 20 seconds.

112

113   This paper gives a discussion and presentation of data on the effect of diurnal variation that are
114 always missed at the local OMI mid-day overpass times. We show that OMI $TCNO_2$ values are also
115 systematically lower than PANDORA values at sites with significant pollution ($TCNO_2 > 0.3$ DU). We present
116 a unique view of a year of fully time resolved diurnal variation of $TCNO_2$ at two sites, Washington DC and
117 New York City, which are similar to other polluted locations.

118

119 **2.0 Brief Instrument Descriptions**

120   For the purposes of $TCNO_2$ retrievals, both OMI and PANDORA are spectrometer-based
121 instruments using nearly the same spectral range and similar spectral resolution (about 0.5 nm). Both use
122 spectral fitting retrieval algorithms that differ (Boersma et al. 2011; Herman et al., 2009) because of the
123 differences between direct-sun viewing retrievals (PANDORA) and above the atmosphere downward
124 viewing retrievals (OMI). The biggest difference is with the respective fields of view, 13 x 24 km^2 at OMI
125 nadir view and larger off-nadir FOV compared to the much smaller PANDORA FOV (1.2^O) measured in m^2
126 with the precise value depending on the NO_2 profile shape and the solar zenith angle. For example, if most
127 of the $TCNO_2$ is located below 2 km, then the PANDORA FOV is approximately given by
128 $(1.2\pi/180)(2/cos(SZA))$, which for SZA = 45° is about 59x59 m^2. If the solar disk (0.5^O) is used as the limiting
129 factor, then the effective FOV is smaller (25x25 m^2).

130 **2.1 OMI**

131   OMI is an east-west side (2600 km) and nadir viewing polar orbiting imaging spectrometer that
132 measures the earth's backscattered and reflected radiation in the range 270 to 500 nm with a spectral
133 resolution of 0.5 nm. The polar orbiting side viewing capabilities produce a pole to pole swath that is about
134 2600 km wide displaced in longitude every 90 minutes by the earth's rotation to provide coverage of
135 nearly the entire sunlit Earth once per day at a 13:30 solar hour equator crossing time with spatial gaps at
136 low latitudes. OMI provides full global coverage every 2 to 3 days. Additional gaps are caused by a problem
137 with the OMI CCD, "row anomaly" (Torres et al., 2018) that effectively reduces the number of near-nadir
138 overpass views. A detailed OMI instrument description is given in Levelt et al. (2006). $TCNO_2$ is determined
139 in the visible spectral range from 405 to 465 nm where the NO_2 absorption spectrum has the maximum
140 spectral structure and where there is little interference from other trace gas species (there is a weak water
141 feature in this range). OMI $TCNO_2$ overpass data are available for many ground sites (currently 719) from
142 the following NASA website. https://avdc.gsfc.nasa.gov/index.php?site=666843934&id=13 (valid as of 16
143 July 2019).

144

145 **2.2 PANDORA**

146

147   PANDORA is a sun-viewing instrument for SZA < 80° that obtains about 4000 spectra for clear-sky
148 views of the sun in 20 seconds for each of two ranges UV (290 – 380 nm using a UV340 bandpass filter)

149 and visible plus UV (280 – 525 nm using no filter). The overall measurement time is about 80 seconds
150 including a 20 second dark-current measurements between each spectral measurement throughout the
151 day. About 4000 clear-sky spectra for the UV and visible portions are separately averaged together to
152 achieve very high signal to noise ratios (SNR). The UV340 filter for UV portion of the spectra reduces stray
153 light effects from the visible wavelength range. A detailed description of PANDORA and its SNR is given
154 in Herman et al., (2009; 2015). The effect of moderate cloud cover (reduction of observed signal by a
155 factor of 8) in the PANDORA FOV on TCNO$_2$ retrievals is small (Herman et al., 2018). Cloud cover also
156 reduces the number of measurements possible in 20 seconds, which potentially increases the noise level.
157 PANDORA is driven by a highly accurate sun tracker that points an optical head at the sun and transmits
158 the received light to an Avantes 2048 x 32 pixel CCD spectrometer (AvaSpec-ULS2048 from 280 – 525 nm
159 with 0.6 nm resolution) through a 50 micron diameter fiber optic cable. The estimated TCNO$_2$ error is
160 approximately 0.05 DU (1 DU = 2.69 x 10^{16} molecules cm^{-2}) out of a typical value of 0.3 DU in relatively
161 clean areas and over 3 DU in highly polluted areas. PANDORA data are available for 250 sites. Some sites
162 have multi-year data sets, but many of these sites are short-term campaign sites.
163 https://avdc.gsfc.nasa.gov/pub/DSCOVR/Pandora/DATA_01/. (valid as of 16 July 2019).
164
165 **3.0 Overpass Comparisons and Diurnal Variation of TCNO$_2$**
166
167   The contribution of NO$_2$ to air quality at the Earth's surface is usually a proportional function of
168 TCNO$_2$ that varies with the time of day and with the altitude profile shape (Lamsal et al., 2013; Bechle et
169 al., 2013). Most of the NO$_2$ amount is usually located between 0 and 3 km altitude with a small amount of
170 about 0.1±0.05 DU (Dirksen et al. 2011) in the upper troposphere and stratosphere. Because of the
171 relatively short chemical lifetime, 3-4 hours (Liu et al., 2016), in the lower atmosphere, most of the NO$_2$ is
172 located near (0 to 20 km) its sources (industrial activity, power generation, and automobile traffic). At
173 higher altitudes or in the winter months, the life time of NO$_2$ is longer permitting transport over larger
174 distances from its sources.
175
176   During the South Korean campaign (KORUS-AQ) in the spring of 2016 the diurnal variations of
177 TCNO$_2$ vs days of the year DOY were determined for 6 sites (Herman et al., 2018), one of which is
178 reproduced here (Fig. 1) for the city of Busan showing relatively low values of TCNO$_2$ in the morning (0.5
179 DU), moderately high values during the middle of the day (1.3 DU), and very high values on some of the
180 afternoons (2 to 3 DU). Of these data, OMI only observes midday values near the 13:30 time marked on
181 the Local_Time axis of Fig.1 thereby missing very high values (2 to 3 DU) that frequently occur later in the
182 afternoon coinciding with times when people are outdoors returning from work.
183
184   In addition to not being designed to observe the TCNO$_2$ diurnal variation, the OMI values are
185 about half those observed by PANDORA (Fig. 2) at the OMI overpass time, so that using OMI values to
186 estimate NO$_2$ pollution seriously underestimates the air quality problem even at midday. The shaded area
187 in Fig.2 corresponds to the period covered in the KORUS-AQ campaign 7 April to 11 June 2016 shown in
188 Fig. 1. An extended time series for Busan location is shown in Fig. 3.
189

190   Because of the different effective NO_2 FOV of PANDORA (measured in m^2) while tracking the
191   moving sun position located in the heart of Busan (FOV distance d < 5 km for an SZA < 70° used for
192    $TCNO_2$ retrievals), both the daily (Fig. 3, left panel) and PANDORA monthly average variation (Fig. 3, right
193   panel), obtained at the OMI overpass time, differs from the variation in the OMI $TCNO_2$ caused by the
194   much larger OMI FOV (13 x 24 km^2 at OMI nadir view) retrieval. Because of this, the OMI time series has
195   low correlation (r^2 = 0.1) with the PANDORA time series.

196

197   The extended OMI vs PANDORA time series from 2012 – 2017 for Busan (Fig. 3) shows the same
198   magnitude of differences seen during the KORUS-AQ period. A similar OMI vs PANDORA plot for total
199   column ozone TCO_3 (Appendix Fig A1) shows good agreement between PANDORA and OMI indicating that
200   the PANDORA instrument was operating and tracking the sun properly. Because the spatial variability of
201   TCO_3, which is mostly in the stratosphere, is much less than for $TCNO_2$, the effect of different FOV's is
202   minimized for ozone.

203

204   The same type of differences, $TCNO_2$(PAN) > $TCNO_2$(OMI), are seen at a wide variety of sites (e.g.,
205   see Fig.4 and Fig. 5) for Northern Hemisphere sites and one site in the Southern Hemisphere where
206   PANDORA has an extended time series. Comparing extended Busan multi-year time series, some broad-
207   scale correlation can be seen with peaks in February 2013, January 2014, and in 2016. The OMI data from
208   Busan are different than data from many sites, since Busan is located very near the ocean causing a portion
209   of the OMI FOV to be over the relatively unpolluted ocean areas, whereas PANDORA is located inland
210   (Pusan University) in an area of dense automobile traffic and quite near mountains capable of trapping
211   air.

212

213   Figures 4 and 5 show a variety of different sites, ranging from the Mauna Loa Observatory location
214   at 3.4 km (11,161 feet) on a relatively clean Hawaiian Island surrounded by ocean to a polluted landlocked
215   semi-arid site at Waterflow, New Mexico near a power plant. All the sites considered show a significant
216   underestimate of OMI $TCNO_2$. A summary of the monthly average underestimates is given in Tables 1 and
217   2. For some sites there is evident correlation between the two offset measurements. For example, the
218   PANDORA at NASA Headquarters in Washington DC tracks the OMI measurement quite well on a monthly
219   average basis with a correlation coefficient of r^2(mn) = 0.7 even though the daily correlation is low (r^2(dy)
220   = 0.17). Other sites have only short periods of correlation and overall weak correlation (Table 1 showing
221   daily, dy and monthly, mn, correlation coefficients for the graphs in Figures 4 and 5)

222

223        $TCNO_2$(PAN) comparisons with $TCNO_2$(OMI) from Mauna Loa Observatory MLO (Fig. 4) are not
224   those that might be expected, since the PANDORA observations are in an area where there are almost no
225   automobile emissions and certainly no power plants, yet PAN > OMI and $TCNO_2$(PAN) values are large
226   enough so that the pollution values (0.18 DU) are well above the stratospheric values (approximately 0.1
227   DU). OMI, which mainly measures values over the clean ocean, has an average value of about 0.1 DU (see
228   appendix Fig. A2). Since there are no emission or combustion sources of NO_2 at high altitudes near MLO
229   at 3.4 km, the PANDORA values suggest upward airflow from the near sea level circumferential ring road,
230   Keahole oil power plant, and resort areas. The Mauna Loa $TCNO_2$ values do not show any correlation with
231   the recent increased volcanic activity at Mt. Kilauea after 2016. A graph showing the mid-day values of

232 TCNO$_2$ at MLO is given in the appendix. Recently, the original Mauna Loa PANDORA has been replaced.
233 The new instrument's calibration will be reviewed before being added to the time series as part of a
234 general data quality assurance program that is starting with the most recently deployed or upgraded
235 PANDORA instruments at about 100 locations.

Table 1 Values of TCNO$_2$ for PANDORA and OMI from monthly averages in Figs. 4 and 5

Name	Location (Lat, Lon)	PAN (DU)	OMI (DU)	r^2 (dy, mn)
Mauna Loa Hawaii	19.536°, -155.5762°	0.16	0.11	0.01, 0.30
NASA HQ Washington DC	38.882°, -77.01°	0.34	0.25	0.17, 0.70
Waterflow New Mexico[1]	36.797°, -108.48°	0.32	0.18	0.13, 0.52
Seoul South Korea	37.5644°, 126.934°	1.2	0.58	0.11, 0.06
Busan South Korea	35.2353°, 129.0825°	0.68	0.32	0.09, 0.10
Boulder Colorado	39.9909°, -105.2607°	0.27	0.17	0.04, 0.09
Buenos Aires Argentina	-34.5554°, -58.5062°	0.50	0.26	0.16, 0.08
Average		**0.49**	**0.27**	

236

Table 2 Average values of TCNO$_2$ for PANDORA and OMI for additional sites

Name	Location (Lat, Lon)	PAN (DU)	OMI (DU)
Essex Maryland	39.31083°, -76.47444°	0.30	0.28
Baltimore Maryland	39.29149°, -76.59646°	0.45	0.27
Fresno California	36.7854°, -119.7731°	0.42	0.17
Denver La Casa Colorado	39.778°, -105.006°	0.68	0.19
GIST[2]	35.226°,126.843°	0.42	0.20
HUFS[3]	37.338°,127.265°	0.61	0.51
City College New York City	40.8153°,-73.9505°	0.60	0.40
Average		**0.50**	**0.29**

[1]Waterflow, NM is listed for OMI data as Four Corners, NM, a nearby landmark
[2]Gwangju Institute of Science and Technology S. Korea
[3]Hankuk University Foreign Studies South Korea

237

238 An interesting inland site is near the very small town of Waterflow, New Mexico (Figs. 4 and 6),
239 where two power plants located near the PANDORA site ceased operation on December 30, 2013
240 (Lindenmaier et al., 2014). According to a quote from AZCentral Newspaper (Tuesday 31 December 2013)
241 "Three coal-fired generators that opened in the 1960s near Farmington, N.M., closed Monday as part of
242 a $182 million plan for Arizona Public Service Co. to meet environmental regulations, the utility reported".
243 The TCNO$_2$ data suggests that the actual shutdown occurred near October 15, 2013. After the shutdown,
244 air quality improved in the area with TCNO$_2$ decreasing from 0.4 DU to 0.28 DU. The remaining more
245 efficient generators continued to produce smaller N0$_2$ emissions. These were shut down at the end of
246 2016 with little additional observed change in TCNO$_2$, since these boilers used NO$_2$ scrubbers (Dubey at
247 al., 2018 in preparation). A nearby highway (Route 64) about 2 km from the PANDORA site has little
248 automobile traffic. An example of the diurnal behavior of TCNO$_2$ at Waterflow, New Mexico on 6 June
249 2012 is shown in Fig. 6 to illustrate the behavior of PANDORA TCNO$_2$ retrievals at a wide range of SZA. The

Table 2 contains a summary of some sites that were part of short-term Discover-AQ campaigns in Maryland, Texas, California, and Colorado, two longer-term sites in South Korea, and one in New York City. Essex, Maryland is located on the Chesapeake Bay 10 km east of the center of Baltimore. The site is relatively clean (PAN = 0.3 DU) compared to the center of Baltimore (PAN = 0.45 DU), while OMI measures about the same amounts for both sites (0.28 and 0.27 DU) because the OMI FOV is larger than the distance between the two sites. The Houston Texas site contains 7 months of data from January to July 2013 with widespread NO_2 pollution permitting PANDORA and OMI to measure the same average values even though PANDORA observes episodes on many days when $TCNO_2$ exceeds 1.5 DU for short periods at times not observed by OMI. Observations in the small city of Fresno, California were during January when agricultural sources of NO_2 were at a minimum (Almaraz, 2018), but automobile traffic in the center of Fresno was significant. In this situation, PANDORA recorded the effect of automobile traffic while OMI averaged the city of Fresno and surrounding fallow agricultural areas. The Denver La Casa location is in the center of the city in an area with high amounts of local automobile traffic and near the Cherokee power generating plant. The result is a high level of average pollution (0.42 DU) while OMI measures both the city center and the surrounding relatively clean plains areas. The HUFS South Korean site is southeast of Seoul in a fairly isolated valley. However, Seoul and its surrounding areas are a widespread transported source of pollution so that both PANDORA and OMI measure elevated $TCNO_2$ amounts. In contrast, the PANDORA GIST site is on the outskirts of a small city in southwestern South Korea with significant traffic. The result is significant amounts of localized $TCNO_2$ (PANDORA = 0.42) surrounded by areas that produce little NO_2 leading to OMI observing a very clean 0.2 DU. The average of sites in the two tables are similar leading to ratios of PAN/OMI of 1.8 and 1.7, respectively. The estimated 50% increase in OMI retrievals of $TCNO_2$ from using the geometry-dependent reflectivity (Vasilkov, 2017) for the most polluted sites will narrow the disagreement with PANDORA. For example, OMI Seoul $TCNO_2$ may become 0.87 DU (PANDORA = 1.2 DU) and Buenos Aires 0.39 DU (PANDORA = 0.5 DU) still underestimating the amount of NO_2 pollution and missing the significant diurnal variation.

292   For the six sites shown, the average OMI underestimate of $TCNO_2$ is approximately a factor of 1.8
293   at the overpass time on a monthly average basis with occasional spikes that exceed this amount. The bias
294   values range from 1.1 to 3.6, with higher biases tending to be associated with higher $TCNO_2$ values. The
295   factor of 1.8 underestimate ignores the frequent large values of $TCNO_2$ at other times during the day (Fig.
296   7). In addition, averaging $TCNO_2$(PAN) over each entire day yields average values for the whole period that
297   are 10 to 20% higher than just averaging over midday values that matched the OMI overpass time. Aside
298   from the absolute magnitude, the short-term variations (over several months) are similar for both OMI
299   and PANDORA although mostly not correlated. If correlation coefficients r^2 are generated from linear fits
300   to scatter plots of $TCNO_2$ from OMI vs PANDORA, the correlation is mostly poor (Examples, r^2 =: Seoul
301   0.06, Mauna Loa 0.3 NASA HQ 0.7, see Figs. 4 and 5). Additional sites with shorter PANDORA time series
302   of $TCNO_2$ show similar behavior.

303   Duncan et al. (2016) estimated trends from OMI $TCNO_2$ time series and found that the Seoul
304   metropolitan area had a decrease of -1.5 ± 1.3 %/Year (2005 – 2014) consistent with OMI estimated
305   change of –1.4 ± 1%/year (2012 -2018) in this paper. However, for the small area near Yonsei University,
306   the decrease estimated from PANDORA is -5.8 ± 0.75 %/Year. Park (2019) estimates that metropolitan
307   Seoul has decreased in population even as surrounding areas have increased population.

308   The average percent differences between OMI and PANDORA shown in Fig. 7 are relatively
309   constant over time for each site with small changes over each multi-year observation period. The
310   differences between OMI and PANDORA are provided by forming the percent differences of the daily
311   $TCNO_2$ values (Fig. 7) in the form 100(OMI – PAN)/PAN. Also shown are the average percent differences
312   and the linear fit slopes in percent change per year of the percent differences over the multi-year period.
313   For example, the Boulder percent difference goes from -31% to -23% over 4 years. Of the six sites in shown
314   in Fig. 7, two have statistically significant slopes, Seoul South Korea 2.1±0.5 %/Year and NASA
315   Headquarters in Washington DC 3.4±0.9 %/Year at the 2σ level suggesting a significant area average
316   increase in pollution compared to PANDORA's local values.

317   For some sites (see Fig. 7), PANDORA and OMI trends are the same within statistical uncertainty
318   (Waterflow, NM, Buenos Aires, and Mauna Loa) while the other 3 sites show significantly different trends
319   (Boulder, NASA HQ, and Seoul).

320   The results for Busan (from Fig. 3) show a least squares average for the percent difference of -48
321   ± 0.8% for the 2012 – 2018 period with a slope of 6.8 ± 1%/Year. There is a decrease in the percent
322   difference after October 2015 (Fig. 3) that is mainly from PANDORA seeing less $TCNO_2$ than during the
323   2012 – 2014 period. There is a gap in the Busan time series from July 2014 until April 2015 when the
324   original PANDORA was replaced with a new instrument. The calibrations of both PANDORAS appear to be
325   correct. Because of the break in the time series it is not clear whether there was a change in local
326   conditions around Pusan University compared to the wide area observed by OMI.

327

328

3.1 Diurnal Variation of TCNO$_2$ Compared to OMI Retrievals

Figure 8 shows details of the daily diurnal variation of TCNO$_2$ on the roof of NASA Headquarters Washington, DC adjacent to a major cross-town highway (I695) for every day during each month of 2015 for local time vs DOY. The midday observing local standard time for OMI is marked for each graph. Displaying an entire year of daily (2-minute time resolution) PANDORA data shows that the high values of TCNO$_2$ are a frequent occurrence but do not occur every day.

The amount of TCNO$_2$ is mostly from the adjacent highway and the surrounding urban area with heavy traffic. The relatively moderate TCNO$_2$ values (0.4 to 0.8 DU) are probably a testament to the effectiveness of catalytic converters mandatory on all US automobiles in such a high traffic area (Bishop and Steadman, 2015). The same data are plotted in Fig. 6 for 8 June 2017 showing that OMI reasonably matched the values seen by PANDORA at 14:00 and 15:00 but was not available to observe high values that occurred in the morning.

Figure 9 contains the daily TCNO$_2$ diurnal variability vs DOY for each month measured by a PANDORA from the roof of a building on the CCNY (City College of New York) campus in the middle of Manhattan in New York City (NYC). From the values shown, the pollution levels are quite high, rivaling the pollution levels in Seoul, South Korea (see Fig. 5). OMI at its mid-day overpass time would detect some of the high-level pollution events, but miss many others occurring mostly in the afternoon. There are a significant number of days in all the months where the TCNO$_2$ levels appear to be low (e.g., blue color in July and October), but the blue color still represents significant pollution levels (TCNO$_2$(PAN) > 0.5 DU) that are small only compared to the peak values during the month (TCNO$_2$(PAN) > 1 DU). The highest amount of TCNO$_2$ recorded during 2018 was about 5DU on 13 July 2018 from 11:20 and 12:30 EST (a time with very light winds (1 km/hr) and moderate temperature (25°C). There were many smaller peaks between 2 and 3 DU throughout the year. Extreme cases of high NO$_2$ amounts are frequently associated with the local meteorology indications of stagnant air (Harkey et al., 2015), The same data are shown in Fig. 6 for two days, 7 May 2018 and 7 June 2018 showing the comparison with OMI and the occurrence of much higher values of TCNO$_2$ in the morning and afternoon.

For both Washington DC (Fig. 8) and New York City (Fig. 9) there is strong day-to-day and month to month variability that depends on the local meteorological conditions (Seo et al., 2018; Zeng et al., 2015) and the amount of automobile traffic in the area (Andersen et al., 2011; Amin et al., 2017). High TCNO$_2$ events occur most often in the afternoon such that the OMI overpass near 13:30 would miss most high TCNO$_2$ events. Poor air quality affecting respiratory health would be improperly characterized by both the OMI average values being too low (Fig. 4) and by missing the extreme pollution events that occur frequently in the late afternoon. The high value of TCNO$_2$ that occurred on 5 August (2.2 DU) at 07:45 EST for Washington DC is not a retrieval error (SZA less than 70°), but is a one-time anomaly in 2015 compared to more usual high values of 1.5 DU with an occasional spike to 2 DU. It should be noted that TCNO$_2$ does not accurately represent the NO$_2$ concentration at the surface, since it is mostly a measure of the amount in the lower 2 km. However, it is roughly proportional to the surface measurements close to the pollution sources (Bechle et al., 2013; Knepp et al., 2014) with the exact proportionality dependent on the profile shape near the ground.

368   Similar daily diurnal variation graphs of TCNO$_2$ (Figs. 8 and 9) could be shown for each site.
369   However, the basic idea is the same for each site. OMI underestimates the amount of TCNO$_2$ because of
370   its large FOV and misses most of the peak events at other times of the day. For some sites, such as Busan
371   and Seoul, the peak values can reach 3 DU and above late in the afternoon, which are never seen by OMI
372   (Herman et al., 2018).

373   Figure 10 for CCNY is similar to the graphs in Figs. 4 – 6 showing the relative behavior between
374   PANDORA and OMI but including only OMI pixels that are at a distance D < 30 km from CCNY. The results
375   are almost identical to those when D < 80 km. There is a period in March 2018 when OMI TCNO$_2$ slightly
376   exceeded that measured by PANDORA. OMI with its large FOV may be seeing part of the chemically driven
377   seasonal variation, while PANDORA is seeing a nearly constant source driven amount mostly from
378   automobile traffic. For most days during 2018, PAN(TCNO$_2$) > OMI(TCNO$_2$) with the average value for PAN
379   = 0.65 DU and for OMI = 0.45 DU (Fig. 10 Panel B). The percent difference plot shows that there is a
380   systematic increase between PANDORA and OMI TCNO$_2$ from a value 10% to a value of 50%.

381

4.0 Summary

383   Examination of long-term TCNO$_2$ monthly average time series from OMI satellite and PANDORA
384   ground-based observations show that OMI systematically underestimates the amount of NO$_2$ in the
385   atmosphere by an average factor of 1.5 to 2 at the local OMI overpass time near the equator crossing time
386   of 13:30±1:30. As shown in Fig. 7 for TCNO$_2$, 100(OMI – PAN)/PAN least squares mean underestimates are
387   much larger than error estimates. These differences are reduced for the smaller pixel size TropOMI TCNO2
388   values (Judd et al.,2019). In addition, the PANDORA diurnal time series for every day during a year at each
389   site (only two typical sites are shown in this paper, NYC and NASA-HQ) shows peaks in TCNO$_2$ that are
390   completely missed by only observing at mid-day (see Figs. 6, 8, 9, and A2). The result is that estimates of
391   air quality related to health effects from OMI observations are strongly underestimated almost
392   everywhere as shown at all the sites with a long PANDORA record. In comparisons to PANDORA, OMI data
393   are mostly uncorrelated or weakly correlated (e.g., Seoul correlation coefficient r^2 = 0.06, Mauna Loa r^2 =
394   0.3), while NASA HQ in Washington, DC shows a correlation on a seasonal basis (NASA HQ r^2 = 0.7)
395   suggesting a wide area coordinated source of NO$_2$ (most likely automobile traffic). The data from CCNY
396   shows some correlation between the locations of the peaks and troughs. Seven short term TCNO$_2$ time
397   series were examined showing similar results (Table 1), except when the pollution region is widespread
398   as in the Seoul South Korea region. The conclusion is that while OMI satellite TCNO$_2$ data are uniquely
399   able to assess regional long-term trends in TCNO$_2$ and provide a measure of the regional distribution of
400   pollutants, the OMI data cannot properly assess local air quality or the effect on human health over
401   extended periods in urban or industrial areas. This will continue to be the case, but to a lesser degree,
402   when the OMI TCNO$_2$ data are improved by reprocessing with a new geometry-dependent reflectivity
403   (Vasilkov, 2017) and by the smaller FOV of TropOMI. The analysis shows that locating PANDORAs at
404   polluted sites could provide quantitative corrections for spatial and temporal biases that affect the
405   determination of local air quality from satellite data. Satellite detection of diurnal variation of TCNO$_2$ will
406   be improved with the upcoming launch of three planned geostationary satellites over Korea, US, and

407 Europe To verify the proper operation of the various PANDORA instruments, a similar analysis for Total
408 Column Ozone TCO was performed (see Appendix) and shows close agreement between OMI and
409 PANDORA, with the largest difference occurring for Mauna Loa Observatory at 3.4 km altitude, where
410 PANDORA misses the ozone between the surface and 3.4 km.

411 **Appendix**

412   **Ozone:** This section shows the corresponding PANDORA total column ozone (TCO) values
413 compared to OMI TCO for Busan South Korea (Fig. A1) that shows close agreement for the entire 2012 –
414 2017 period. The different fields of view for OMI and PANDORA have a much smaller effect because of
415 the greater spatial uniformity of stratospheric ozone compared to tropospheric NO_2. Additional sites are
416 summarized in Table A1. The largest TCO difference (15 DU or 5.6%) occurs for Mauna Loa Observatory
417 (Altitude = 3.4 km) compared to OMI (Average altitude = Sea Level). The close results show that the
418 PANDORA was working properly and pointing accurately at the sun. The PANDORA TCO data shown here
419 use a mid-latitude effective ozone temperature correction from model calculations that may not be
420 accurate of each individual site (Herman et al., 2017). The ozone retrievals shown here use an average
421 effective ozone temperature instead of a locally measured ozone temperature (Herman et al.,
422 2015;2017).

423

424

Table A1 Average values of TCO_3 for PANDORA and OMI

Location	PAN (DU)	OMI (DU)	Percent Difference
Mauna Loa Observatory Hawaii (3.394 km)*	254	269	5.6
NASA HQ Washington DC (0.02 km)	308	314	1.9
Waterflow New Mexico (1.64 km)	293	292	0.3
Yonsei University Seoul South Korea (0.07 km)	317	325	2.5
Busan University Busan South Korea(0.03 km)	313	315	0.6
Boulder, Colorado (NOAA Bldg) (1.617 km)	299	302	1.0
Buenos Aires, Argentina (0.025 km)	279	284	1.8
Essex, Maryland (0.012 km)	299	301	0.7
Baltimore, Maryland (0.01 km)	296	296	0.0
Fresno, California (0.939 km)	306	309	1.0
Denver La Casa Colorado (1.6 km)	292	294	0.7
Gwangju Institute of Science and Technology (GIST) S. Korea (0.021 km)	302	307	1.6
Hankuk University Foreign Studies (HUFS) South Korea (0.04 km)	318	326	2.5
City College Manhattan New York City (0.04 km)	316	325	2.8
Average	**299**	**304**	**1.6**

425

426   **Mauna Loa TCNO$_2$**: Figure A2 shows the diurnal variation of TCNO2 at MLO on specific days
427 3,4,7, and 8 of June 2016 along with the variation in SZA. This shows that the MLO is polluted by NO_2

428 with column amounts in excess of stratospheric amounts (approximately 0.1 DU) even though there are
429 no local sources. OMI retrievals of TCNO2 on each day are much lower (about 0.12 DU) because of the
430 averaging over OMI's large FOV that includes very clean ocean areas.

431

432

433

434

435

436

437 **Acknowledgement:** This project is supported by the Korea Ministry of Environment (MOE) as Public Technology
438 Program based on Environmental Policy (2017000160001), by the Los Alamos National Laboratory's Laboratory
439 Directed Research and Development program and by the NASA Pandora project managed by Dr. Robert
440 Swap.

References

Almaraz, Maya,Edith Bai, Chao Wang, Justin Trousdel, Stephen Conley, Ian Faloona and Benjamin Z. Houlton, Agriculture is a major source of NOx pollution in California, SCIENCE ADVANCES,31, DOI:10.1126/sciadv.aao3477, 2018.

Amin, Md. Shohel Reza, Umma Tamima, and Luis Amador Jimenez, "Understanding Air Pollution from Induced Traffic during and after the Construction of a New Highway: Case Study of Highway 25 in Montreal," Journal of Advanced Transportation, vol. 2017, Article ID 5161308, 14 pages, 2017. https://doi.org/10.1155/2017/5161308, 2017.

Andersen, M. Hvidberg, S.S. Jensen, M. Ketzel, S. Loft, M. Sørensen, A. Tjønneland, K. Overvad, O. Raasc hou-Nielsen Chronic obstructive pulmonary disease and long-term exposure to traffic-related air pollution: A cohort study, Am. J. Respir. Crit. Care Med., 183, pp. 455-461, 10.1164/rccm.201006-0937OC, 2011.

Bechle, M. J.; Millet, D. B.; Marshall, J. D. Remote sensing of exposure to NO_2: Satellite versus ground-based measurement in a large urban area. Atmos. Environ., 69, 345-353, 2013

Bishop, Gary A. and Donald H. Stedman, Reactive Nitrogen Species Emission Trends in Three Light-/Medium-Duty United States Fleets, *Environmental Science & Technology* 2015 *49* (18), 11234-11240, DOI: 10.1021/acs.est.5b02392, 2015.

Boersma, K. F., H. J. Eskes, E. J. Brinksma, Error analysis for tropospheric NO_2 retrieval from space, J. Geophys. Res. Atmos., https://doi.org/10.1029/2003JD003962, 2004.

Boersma, K. F., Eskes, H. J., Dirksen, R. J., van der A, R. J., Veefkind, J. P., Stammes, P., Huijnen, V., Kleipool, Q. L., Sneep, M., Claas, J., Leitão, J., Richter, A., Zhou, Y., and Brunner, D.: An improved tropospheric NO_2 column retrieval algorithm for the Ozone Monitoring Instrument, Atmos. Meas. Tech., 4, 1905-1928, https://doi.org/10.5194/amt-4-1905-2011, 2011.

Boersma, K. F., Vinken, G. C. M., & Eskes, H. J., Representativeness errors in comparing chemistry transport and chemistry climate models with satellite UV–Vis tropospheric column retrievals. Geoscientific Model Development, 9(2), 875-898, 2016.

Choudhari, Sheetal Korde, Minal Chaudhary, Sachin Bagde, Amol R Gadbai and Vaishali Joshi, Nitric oxide and cancer: a review, World Journal of Surgical Oncology 2013, 11:118, http://www.wjso.com/content/11/1/118, 2013.

Cleveland, William S., *LOWESS: A program for smoothing scatterplots by robust locally weighted regression. The American Statistician. **35** (1): 54.* JSTOR 2683591*. doi:10.2307/2683591, 1981.*

480   Dirksen, Ruud J., K. Folkert Boersma, Henk J. Eskes, Dmitry V. Ionov, Eric J. Bucsela, Pieternel F. Levelt,
481   Hennie M. Kelder, Evaluation of stratospheric NO2 retrieved from the Ozone Monitoring Instrument:
482   Intercomparison, diurnal cycle, and trending, J. Geophys. Res., 116,
483   https://doi.org/10.1029/2010JD014943, 2011.

484

485   Duncan, B. N., L. N. Lamsal, A. M. Thompson, Y. Yoshida, Z. Lu, D. G. Streets, M. M. Hurwitz, and K. E.
486   Pickering, A space-based, high-resolution view of notable changes in urban NOx pollution around the
487   world (2005–2014), J. Geophys. Res. Atmos.,121, 976–996, doi:10.1002/2015JD024121, 2016.

488

489   Goldberg, D. L., Saide, P. E., Lamsal, L. N., de Foy, B., Lu, Z., Woo, J.-H., Kim, Y., Kim, J., Gao, M., Carmichael,
490   G., and Streets, D. G.: A top-down assessment using OMI NO2 suggests an underestimate in the NOx
491   emissions inventory in Seoul, South Korea during KORUS-AQ, Atmos. Chem. Phys. Discuss.,
492   https://doi.org/10.5194/acp-2018-678, in review, 2018.

493

494   Harkey, M., Holloway, T., Oberman, J., and Scotty, E., An evaluation of CMAQ NO2 using observed
495   chemistry-meteorology correlations, J. Geophys. Res. Atmos., 120, 11,775– 11,797,
496   doi:10.1002/2015JD023316, 2015.

497

498   Herman, J., A. Cede, E. Spinei, G. Mount, M. Tzortziou, and N. Abuhassan, NO2 column amounts from
499   ground-based Pandora and MFDOAS spectrometers using the direct-sun DOAS technique:
500   Intercomparisons and application to OMI validation, J. Geophys. Res., 114, D13307,
501   doi:10.1029/2009JD011848, 2009.

502

503   Herman, J.R., R.D. Evans, A. Cede, N.K. Abuhassan, I. Petropavlovskikh, and G. McConville, Comparison
504   of Ozone Retrievals from the Pandora Spectrometer System and Dobson Spectrophotometer in Boulder
505   Colorado, Atmos. Meas. Tech., 8, 3407–3418, 2015 doi:10.5194/amt-8-3407-2015.

506
507   Herman, J., Evans, R., Cede, A., Abuhassan, N., Petropavlovskikh, I., McConville, G., Miyagawa, K., and
508   Noirot, B.: Ozone comparison between Pandora #34, Dobson #061, OMI, and OMPS in Boulder,
509   Colorado, for the period December 2013–December 2016, Atmos. Meas. Tech., 10, 3539-3545,
510   https://doi.org/10.5194/amt-10-3539-2017, 2017.

511

512   Herman, J., Spinei, E., Fried, A., Kim, J., Kim, J., Kim, W., Cede, A., Abuhassan, N., and Segal-Rozenhaimer,
513   M.: NO$_2$ and HCHO measurements in Korea from 2012 to 2016 from Pandora spectrometer instruments
514   compared with OMI retrievals and with aircraft measurements during the KORUS-AQ campaign, Atmos.
515   Meas. Tech., 11, 4583-4603, https://doi.org/10.5194/amt-11-4583-2018, 2018.

516

517   Ialongo, I., Herman, J., Krotkov, N., Lamsal, L., Boersma, K. F., Hovila, J., and Tamminen, J.: Comparison of
518   OMI NO$_2$observations and their seasonal and weekly cycles with ground-based measurements in Helsinki,
519   Atmos. Meas. Tech., 9, 5203-5212, https://doi.org/10.5194/amt-9-5203-2016, 2016.

520

521   Judd, Laura M., Jassim A. Al-Saadi, Lukas C. Valin, R. Bradley Pierce, Kai Yang, Scott J. Janz, Matthew G.
522   Kowalewski, James J. Szykman, Martin Tiefengraber, and Moritz Mueller, The Dawn of Geostationary Air

Quality Monitoring: Case Studies From Seoul and Los Angeles, Environ. Sci.,https://doi.org/10.3389/fenvs.2018.00085, 2018.

Judd, L. M., Al-Saadi, J. A., Janz, S. J., Kowalewski, M. G., Pierce, R. B., Szykman, J. J., Valin, L. C., Swap, R., Cede, A., Mueller, M., Tiefengraber, M., Abuhassan, N., and Williams, D.: Evaluating the impact of spatial resolution on tropospheric NO_2 column comparisons within urban areas using high-resolution airborne data, Atmos. Meas. Tech. Discuss., https://doi.org/10.5194/amt-2019-161, in review, 2019.

Kleipool, Q.L., M.R. Dobber, J.F. De Haan and P.F. Levelt, Earth Surface Reflectance Climatology from Three Years of OMI Data, Journal of Geophysical Research, 113, doi:10.1029/2008JD010290, 2008.

Knepp, T., M. Pippin, J. Crawford, Jim Szykman, R. Long, L. Cowen, A. Cede, N. Abuhassan, J. Herman, R. Delgado, J. Compton, T. Berkoff, J. Fishman, D. Martins, R. Stauffer, A. Thompson, A. Weinheimer, D. Knapp, D. Montzka, D. Lenschow, AND D. Neil. Estimating Surface NO2 and SO2 Mixing Ratios from Fast-Response Total Column Observations and Potential Application to Geostationary Missions. JOURNAL OF ATMOSPHERIC CHEMISTRY. Springer, New York, NY, 0(0):1-26, (2014).

Kollonige, D. E., Thompson, A. M.,Josipovic, M., Tzortziou, M., Beukes, J. P.,Burger, R., … Laakso, L. (2018). OMI satellite and ground-based Pandora observations and their application to surface NO2 estimations at terrestrial and marine sites. Journal of Geophysical Research: Atmospheres, 123, 1441–1459. https://doi.org/10.1002/2017JD026518, 2018.

Krotkov, N. A., Lamsal, L. N., Celarier, E. A., Swartz, W. H., Marchenko, S. V., Bucsela, E. J., Chan, K. L., Wenig, M., and Zara, M.: The version 3 OMI NO_2 standard product, Atmos. Meas. Tech., 10, 3133-3149, https://doi.org/10.5194/amt-10-3133-2017, 2017.

Lamsal, L & Martin, Randall & Parrish, David & Krotkov, Nickolay., Scaling Relationship for NO_2 Pollution and Urban Population Size: A Satellite Perspective. Environmental science & technology. 47. 10.1021/es400744g, 2013.

Lamsal, L. N., Krotkov, N. A., Celarier, E. A., Swartz, W. H., Pickering, K. E., Bucsela, E. J., Martin, R. V., Philip, S., Irie, H., Cede, A., Herman, J., Weinheimer, A., Szykman, J. J., and Knepp, T. N.: Evaluation of OMI operational standard NO_2 column retrievals using in situ and surface-based NO_2 observations, Atmos. Chem. Phys. Discuss., 14, 14519-14573, doi:10.5194/acpd-14-14519-2014, 2014.

Lamsal, L. N., S. J. Janz, N. A. Krotkov, K. E. Pickering, R. J. D. Spurr, M. G. Kowalewski, C. P. Loughner, J. H. Crawford, W. H. Swartz, and J. R. Herman, High-resolution NO_2 observations from the Airborne Compact Atmospheric Mapper Retrieval and validation, J. Geophys. Res. Atmos., 122, 1953–1970, doi:10.1002/2016JD025483, 2017

Levelt, P. F., Van den Oord, G. H. J., Dobber, M. R., Malkki, A., Visser, H., de Vries, J., Stammes, P., Lundell, J. O. V., and Saari, H.: The Ozone Monitoring Instrument, IEEE T. Geosci. Remote, 44, 1093–1101, doi:10.1109/tgrs.2006.872333, 2006.

Lindenmaier, Rodica, Manvendra K. Dubey, Bradley G. Henderson, Zachary T. Butterfield, Jay R. Herman, Thom Rahn · S.-H. Lee, Multiscale observations of CO2, (CO2)-C-13, and pollutants at Four Corners for emission verification and attribution, Proceedings of the National Academy of Sciences 06/2014; 111(23):8386-8391. DOI:10.1073/pnas.132188311, 2014

Liu, F., Beirle, S., Zhang, Q., Dörner, S., He, K., and Wagner, T.: NO_x lifetimes and emissions of cities and power plants in polluted background estimated by satellite observations, Atmos. Chem. Phys., 16, 5283-5298, https://doi.org/10.5194/acp-16-5283-2016, 2016.

Lorente, A., Boersma, K. F., Stammes, P., Tilstra, L. G., Richter, A., Yu, H., Kharbouche, S., and Muller, J.-P.: The importance of surface reflectance anisotropy for cloud and NO_2 retrievals from GOME-2 and OMI, Atmos. Meas. Tech., 11, 4509-4529, https://doi.org/10.5194/amt-11-4509-2018, 2018.

Nowlan, C. R., Liu, X., Leitch, J. W., Chance, K., González Abad, G., Liu, C., Zoogman, P., Cole, J., Delker, T., Good, W., Murcray, F., Ruppert, L., Soo, D., Follette-Cook, M. B., Janz, S. J., Kowalewski, M. G., Loughner, C. P., Pickering, K. E., Herman, J. R., Beaver, M. R., Long, R. W., Szykman, J. J., Judd, L. M., Kelley, P., Luke, W. T., Ren, X., and Al-Saadi, J. A.: Nitrogen dioxide observations from the Geostationary Trace gas and Aerosol Sensor Optimization (GeoTASO) airborne instrument: Retrieval algorithm and measurements during DISCOVER-AQ Texas 2013, Atmos. Meas. Tech., 9, 2647-2668, https://doi.org/10.5194/amt-9-2647-2016, 2016.

O'Byrne, G., R. V. Martin,A. van Donkelaar, J. Joiner, and E. A. Celarier, Surface reflectivity from the Ozone Monitoring Instrument using the Moderate Resolution Imaging Spectroradiometer to eliminate clouds: Effects of snow on ultraviolet and visible trace gas retrievals, J. Geophys. Res., VOL. 115, D17305, doi:10.1029/2009JD013079, 2010.

Marchenko, S., N. A. Krotkov, L. N. Lamsal, E. A. Celarier, W. H. Swartz, and E. J. Bucsela, Revising the slant column densityretrieval of nitrogen dioxide observed by the Ozone Monitoring Instrument, J. Geophys. Res. Atmos., 120, 5670–5692, doi:10.1002/2014JD022913, 2015

Park, Se Hoon, Seoul, The Wiley Blackwell Encyclopedia of Urban and Regional Studies. Edited by Anthony Orum. John Wiley & Sons Ltd. Published 2019 by John Wiley & Sons Ltd. DOI: 10.1002/9781118568446.eurs0283, 2019.

Raponi, Marcelo, Cede, A, Santana Diaz, Daniel, Sanchez, R, A. Otero, L, O. Salvador, J, R. Ristori, P, Quel, Eduardo. Total Column Ozone Measured In Buenos Aires Between March And November 2017, Using A Pandora Spectrometer System. Anales AFA. 29(2), 46-50. 10.31527/analesafa.2018.29.2.46, 2018.

Seo, J., Park, D.-S. R., Kim, J. Y., Youn, D., Lim, Y. B., and Kim, Y.: Effects of meteorology and emissions on urban air quality: a quantitative statistical approach to long-term records (1999–2016) in Seoul, South Korea, Atmos. Chem. Phys., 18, 16121-16137, https://doi.org/10.5194/acp-18-16121-2018, 2018.

609   Torres, O., Bhartia, P. K., Jethva, H., and Ahn, C.: Impact of the ozone monitoring instrument row
610   anomaly on the long-term record of aerosol products, Atmos. Meas. Tech., 11, 2701-2715,
611   https://doi.org/10.5194/amt-11-2701-2018, 2018.
612
613   Tzortziou, M.; Parker, O.; Lamb, B.; Herman, J.R.; Lamsal, L.; Stauffer, R.; Abuhassan, N. Atmospheric
614   Trace Gas (NO_2 and O_3) Variability in South Korean Coastal Waters, and Implications for Remote
615   Sensing of Coastal Ocean Color Dynamics. *Remote Sens.*, *10*, 1587, ; doi:10.3390/rs10101587, 2018.
616
617   Vasilkov, A., Qin, W., Krotkov, N., Lamsal, L., Spurr, R., Haffner, D., Joiner, J., Yang, E.-S., and Marchenko,
618   S.: Accounting for the effects of surface BRDF on satellite cloud and trace-gas retrievals: a new approach
619   based on geometry-dependent Lambertian equivalent reflectivity applied to OMI algorithms, Atmos.
620   Meas. Tech., 10, 333-349, https://doi.org/10.5194/amt-10-333-2017, 2017.
621
622   Zara, M., Boersma, K. F., De Smedt, I., Richter, A., Peters, E., van Geffen, J. H. G. M., Beirle, S.,
623   Wagner, T., Van Roozendael, M., Marchenko, S., Lamsal, L. N., and Eskes, H. J.: Improved slant column
624   density retrieval of nitrogen dioxide and formaldehyde for OMI and GOME-2A from QA4ECV:
625   intercomparison, uncertainty characterization, and trends, Atmos. Meas. Tech., 11, 4033-4058,
626   https://doi.org/10.5194/amt-11-4033-2018, 2018.
627
628   Zheng, G. J., Duan, F. K., Su, H., Ma, Y. L., Cheng, Y., Zheng, B., Zhang, Q., Huang, T., Kimoto, T., Chang,
629   D., Pöschl, U., Cheng, Y. F., and He, K. B.: Exploring the severe winter haze in Beijing: the impact of
630   synoptic weather, regional transport and heterogeneous reactions, Atmos. Chem. Phys., 15, 2969–
631   2983, https://doi.org/10.5194/acp-15-2969-2015, 2015.
632
633
634

635 **Figure Captions**

636 Fig 1 Diurnal variation of $TCNO_2$ measured at Pusan University in Busan South Korea

637 Fig. 2. Monthly average values of $TCNO_2$ for OMI and PANDORA at OMI overpass times

638 Fig. 3 Extended time series for Busan. Left Panel: individual matching PANDORA and OMI data
639 points for the overpass time ± 6 minutes. Right Panel: monthly averages.

640 Fig. 4. PANDORA compared to OMI. Extended $TCNO_2$ overpass time series for Mauna Loa
641 Observatory, Hawaii, NASA Headquarters, Washington DC, and Waterflow, New Mexico.

642 Fig. 5. PANDORA compared to OMI. Extended $TCNO_2$ overpass time series for Seoul South Korea,
643 Boulder, Colorado, and Buenos Aires, Argentina (Raponi et al. 2018).

644 Fig.6 Diurnal variation of $TCNO_2$ on a single day 1) Two km north of Waterflow, NM near a
645 power plant, 2) On the roof of NASA Headquarters Washington, DC and 3) On the roof or a
646 building at CCNY City College of New York, New York City

647 Fig. 7 Percent differences between OMI and PANDORA. The slopes are the absolute change in the
648 percent difference. For example, the Boulder percent difference goes from -31% to -23% over 4 years.
649 The LS Means are least squares means with the corresponding error estimates

650 Fig. 8A $TCNO_2$ diurnal variation (DU) from January to June, NASA Headquarters Washington, DC
651 from January 2015 to June 2015. The approximate OMI overpass time near 13:30 hours is marked.

652 Fig. 8B $TCNO_2$ diurnal variation (DU) from July to December, NASA Headquarters Washington, DC from
653 July 2015 to December 2015. The approximate OMI overpass time near 13:30 hours is marked

654 Fig. 9A $TCNO_2$ diurnal variation (DU) at CCNY in New York City January to June 2018. The approximate
655 OMI overpass time near 13:30 hours is marked.

656 Fig. 9B $TCNO_2$ diurnal variation at CCNY in New York City July to December 2018. The peak near 5 DU
657 occurs on 13 July 2018 between 11:20 and 12:30 EST. The approximate OMI overpass time near 13:30
658 hours is marked.

659 Fig. 10 $TCNO_2$ overpass time series for CCNY in Manhattan, New York City. Panel A: OMI
660 overpass $TCNO_2$ (Black) compare with OMI (Red). Panel B: Monthly Lowess(0.08) fit to the daily
661 overpass data. Panel C: Percent difference 100(OMI – PAN)/PAN calculated from the data in
662 Panel A

663 Fig. A1 Monthly average values of TCO for OMI and PANDORA at OMI overpass times for Busan South
664 Korea. Shaded area represents the KORUS-AQ campaign period.

665   Fig. A2. The diurnal variation of $TCNO_2$ at MLO on 4 days during June 2016 compared to OMI $TCNO_2$
666   (small square). Shaded areas represent high SZA conditions where the PANDORA retrievals are not
667   accurate.
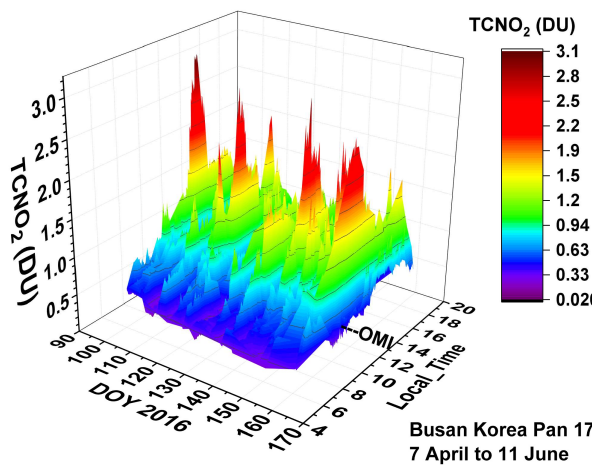
Fig 1 Diurnal variation of TCNO$_2$ measured
at Pusan University in Busan South Korea
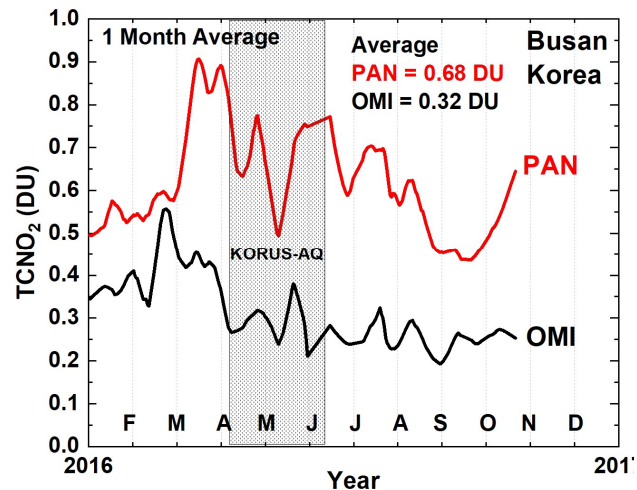
Fig. 2. Monthly average values of TCNO$_2$ for
OMI and PANDORA at OMI overpass times

668

669

670

FIGURE 1   **FIGURE 2**

672

673
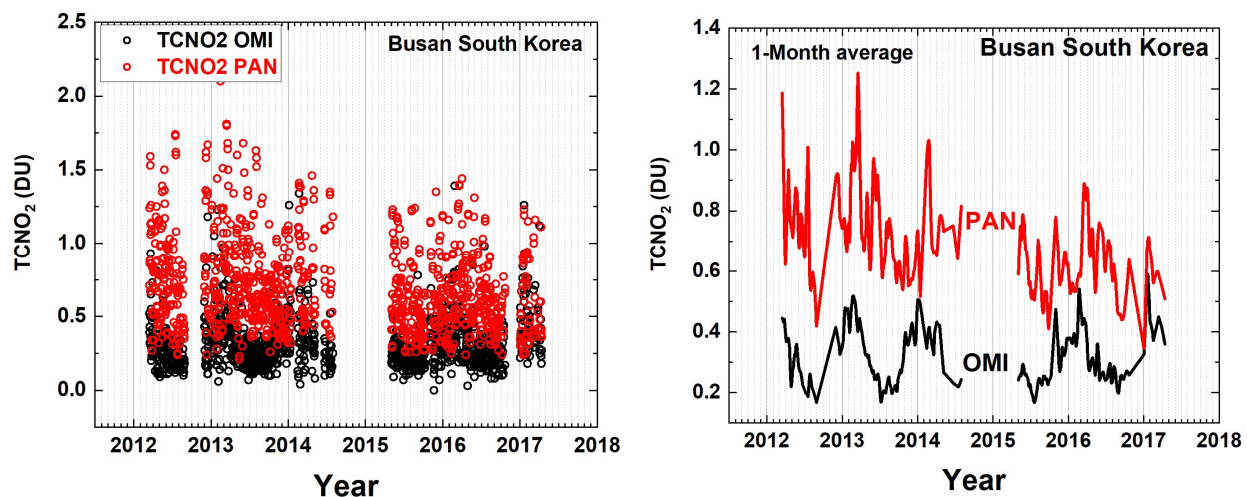
Fig. 3 Extended time series for Busan. Left Panel: individual matching PANDORA and OMI data points for the overpass time ± 6 minutes. Right Panel: monthly averages.

674

675

676 **FIGURE 3**

677
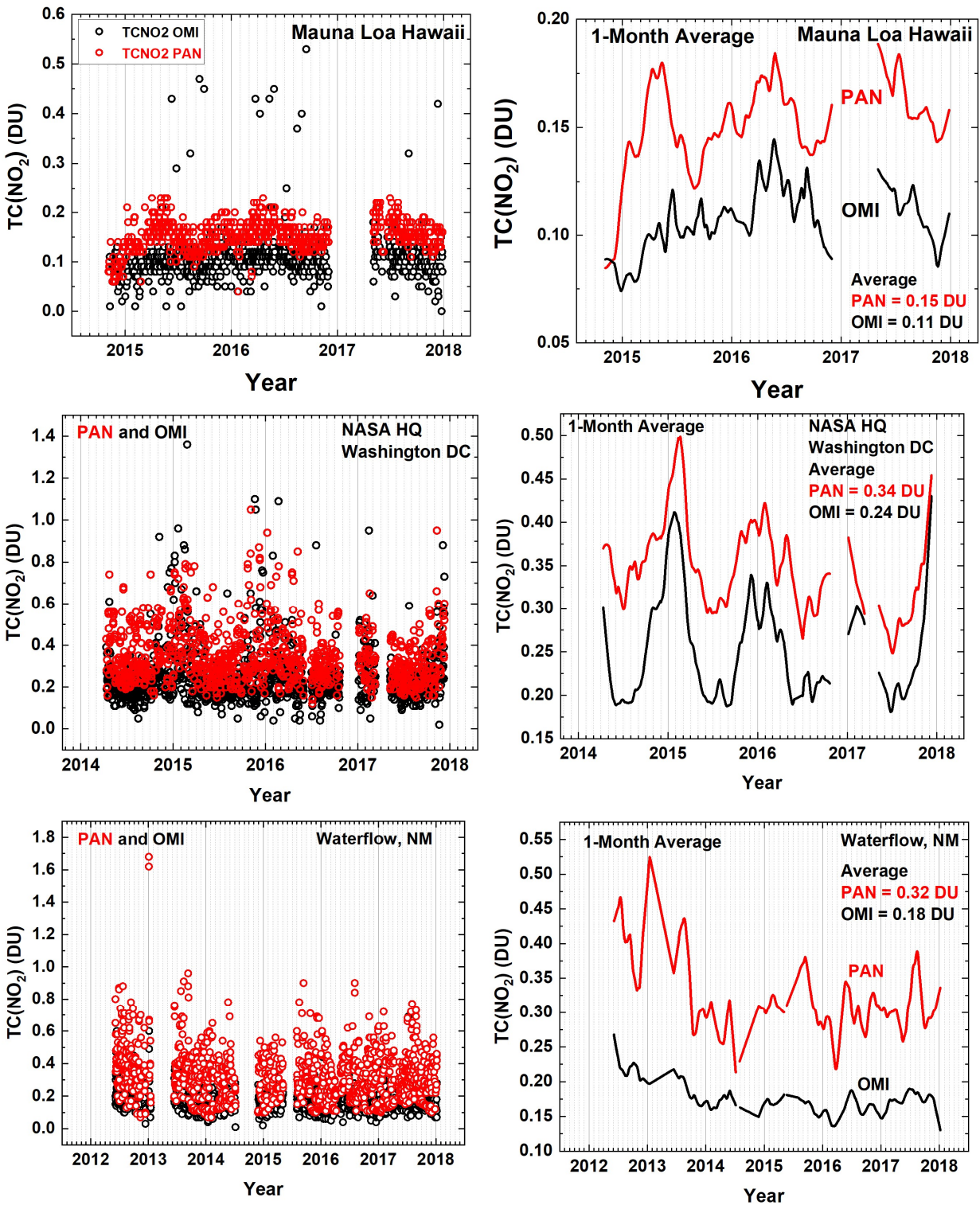
Fig. 4. PANDORA compared to OMI. Extended TCNO₂ overpass time series for Mauna Loa Observatory, Hawaii, NASA Headquarters, Washington DC, and Waterflow, New Mexico.

678 **FIGURE 4**
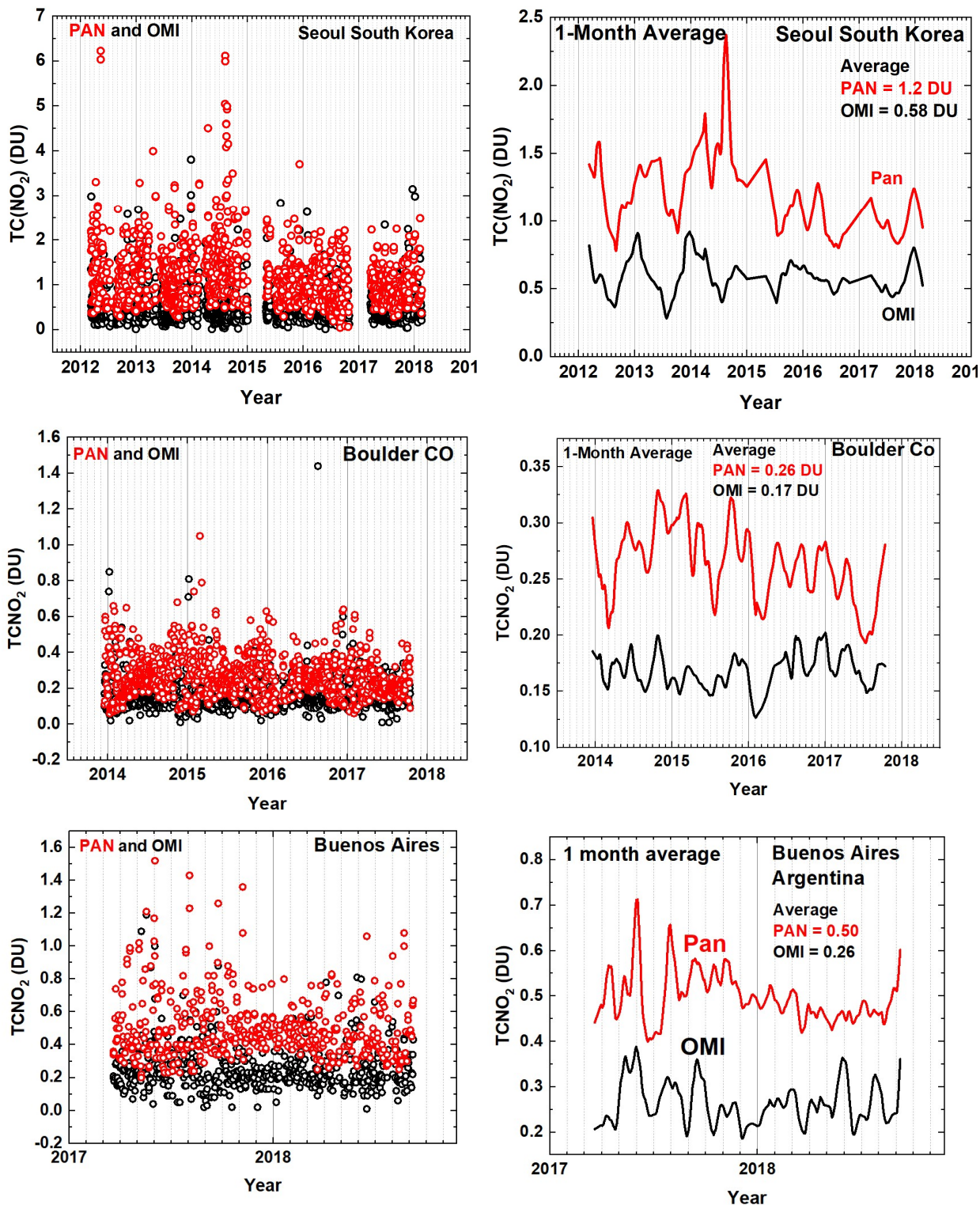
Fig. 5. PANDORA compared to OMI. Extended $TCNO_2$ overpass time series for Seoul South Korea, Boulder, Colorado, and Buenos Aires, Argentina (Raponi et al. 2017).

679 **FIGURE 5**
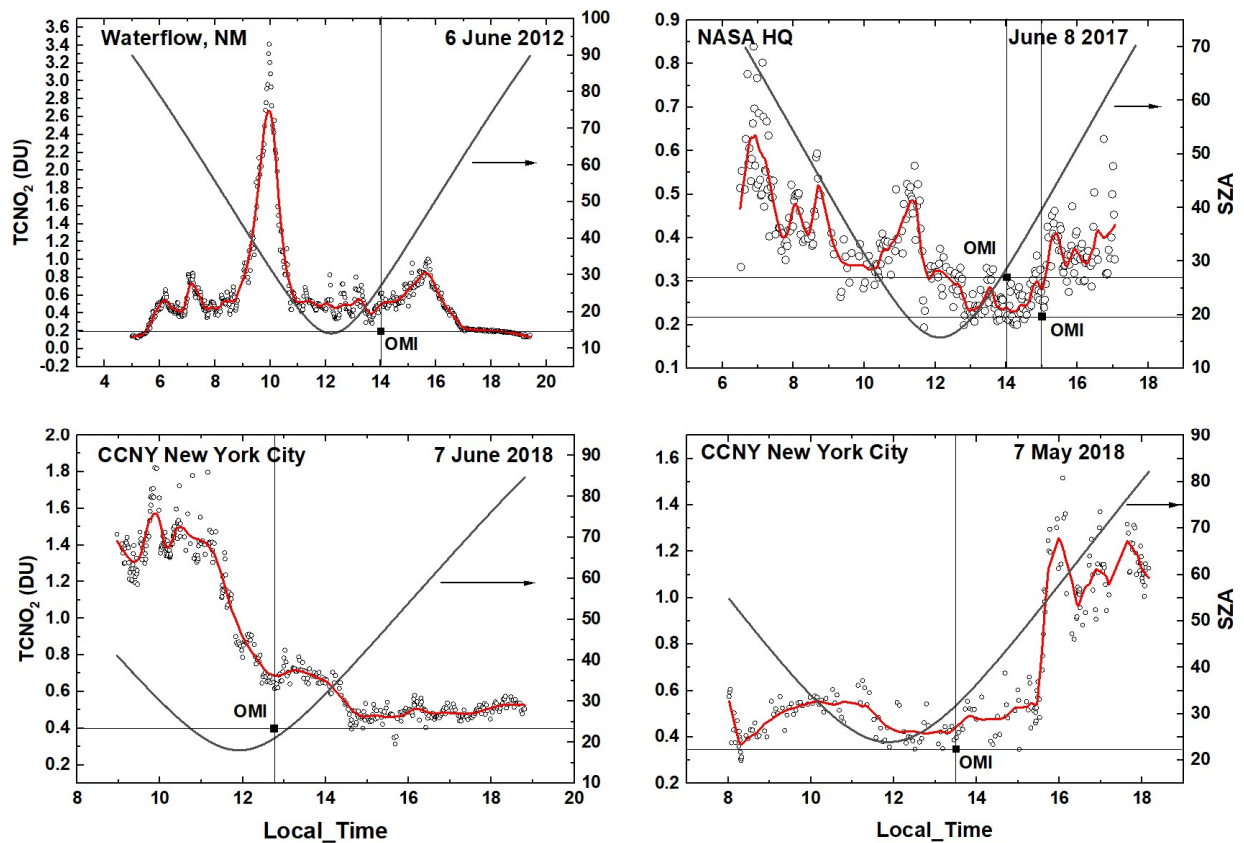
Fig.6 Diurnal variation of TCNO$_2$ on a single day 1) Two km north of Waterflow, NM near a power plant, 2) On the roof of NASA Headquarters Washington, DC and 3) On the roof or a building at City College of New York, New York City

680

681

682

683

684

685   **FIGURE 6**

686

687

688

689

690
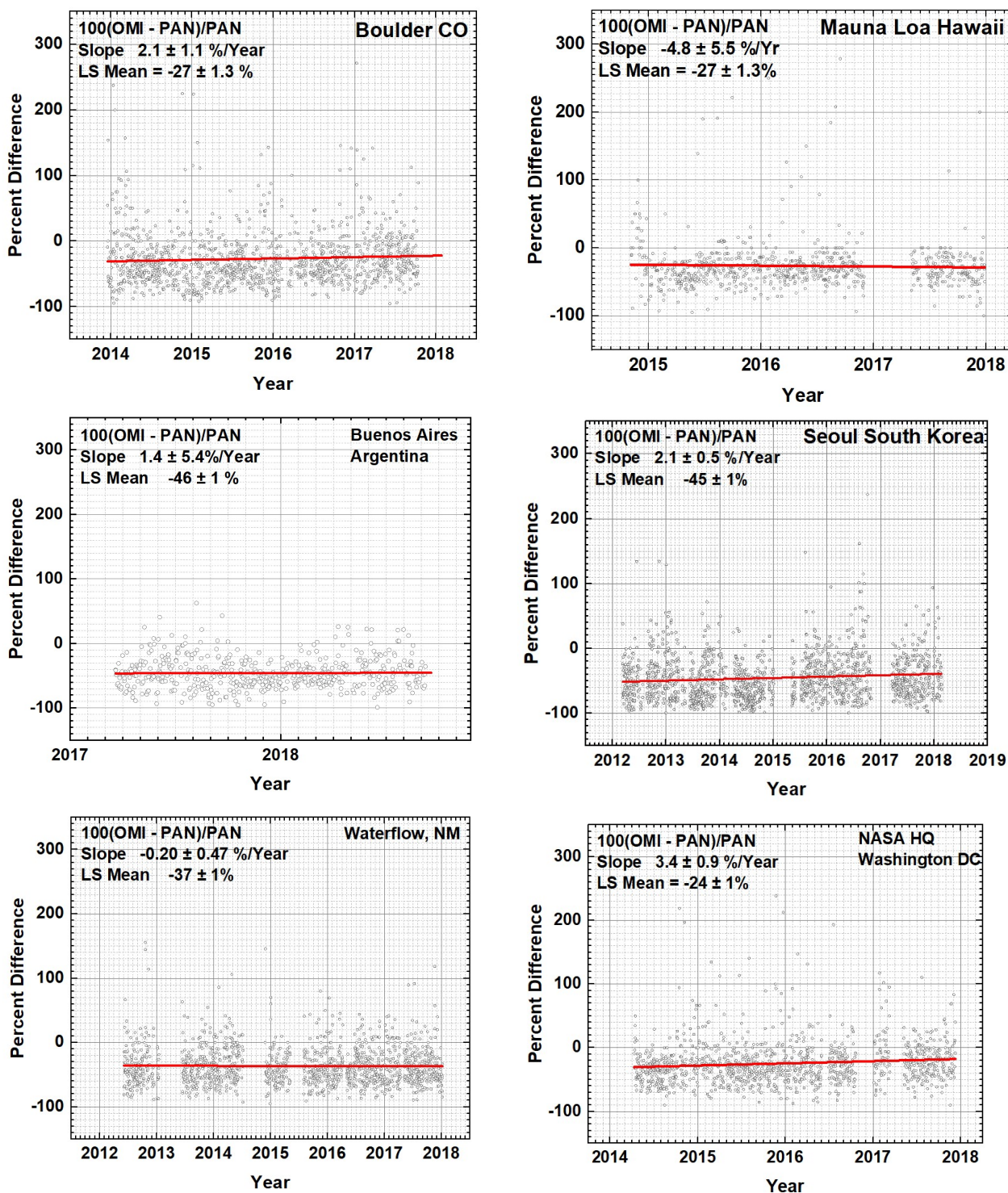
Fig. 7 Percent differences between OMI and PANDORA. The slopes are the absolute change in the percent difference. For example, the Boulder percent difference goes from -31% to -23% over 4 years. The LS Means are least squares means with the corresponding error estimates
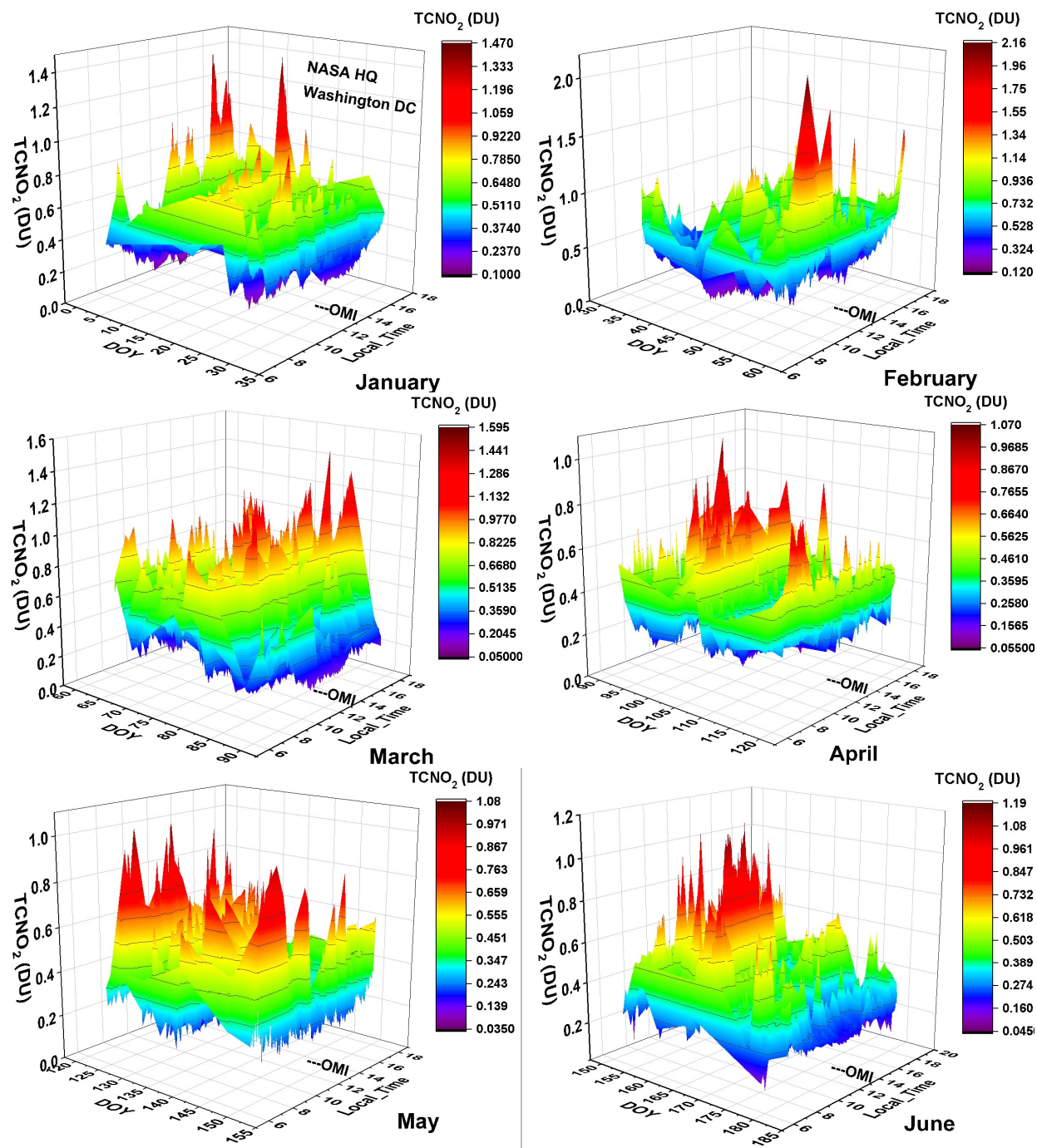
FIGURE 7

691

Fig. 8A TCNO₂ diurnal variation (DU) from January to June, NASA Headquarters Washington, DC from January 2015 to June 2015. The approximate OMI overpass time near 13:30 hours is marked
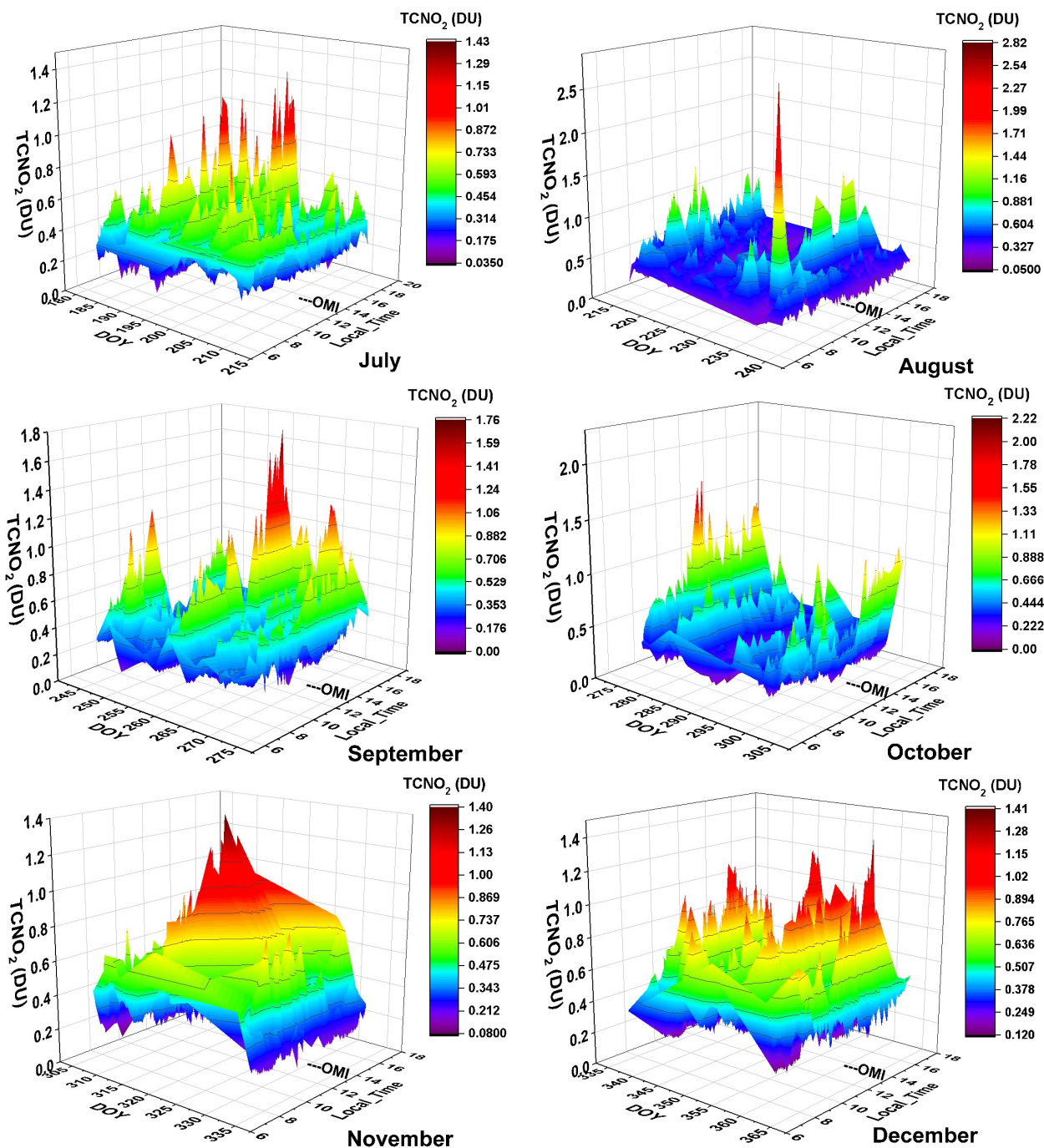
692

FIGURE 8A

Fig. 8B TCNO₂ diurnal variation (DU) from July to December, NASA Headquarters Washington, DC from July 2015 to December 2015. The approximate OMI overpass time near 13:30 hours is marked.

693

FIGURE 8B

694

695
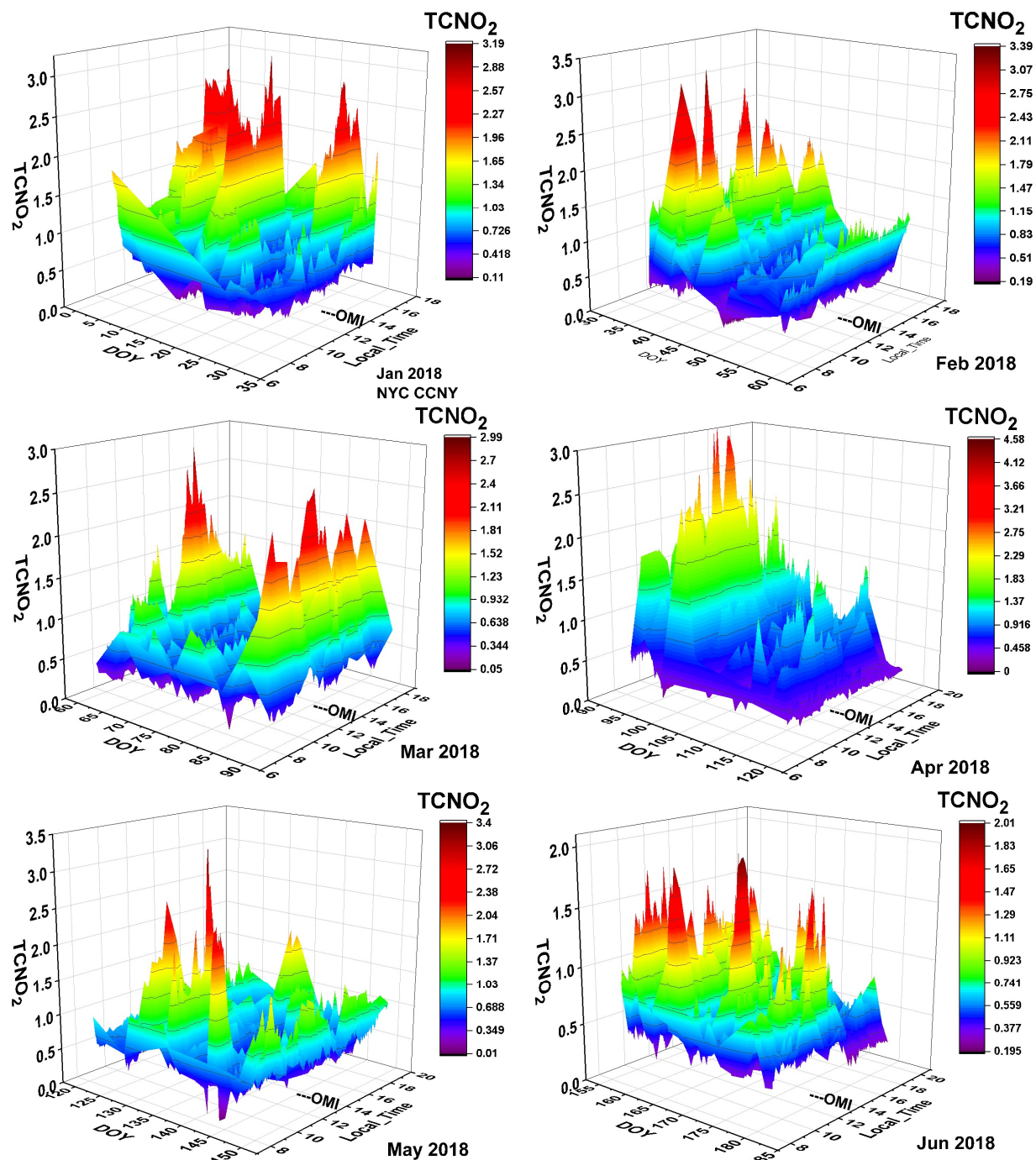
Fig. 9A TCNO$_2$ diurnal variation (DU) at CCNY in New York City January to June 2018. The approximate OMI overpass time near 13:30 hours is marked

696

697 **Figure 9A**
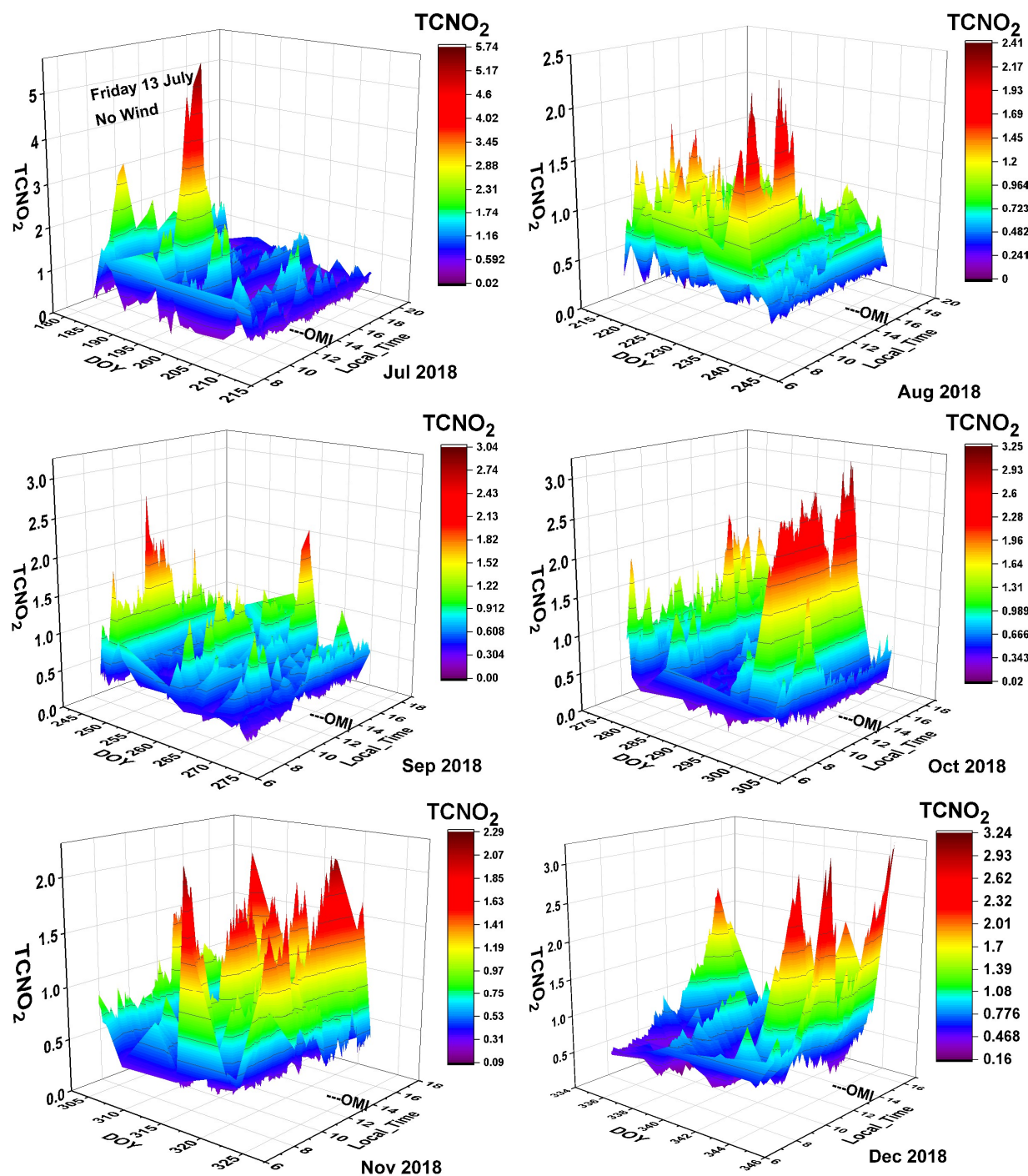
Fig. 9B TCNO₂ diurnal variation (DU) at CCNY in New York City July to December 2018. The peak near 5 DU occurs on 13 July 2018 between 11:20 and 12:30 EST. The approximate OMI overpass time near 13:30 hours is marked.

698

699 **Figure 9B**
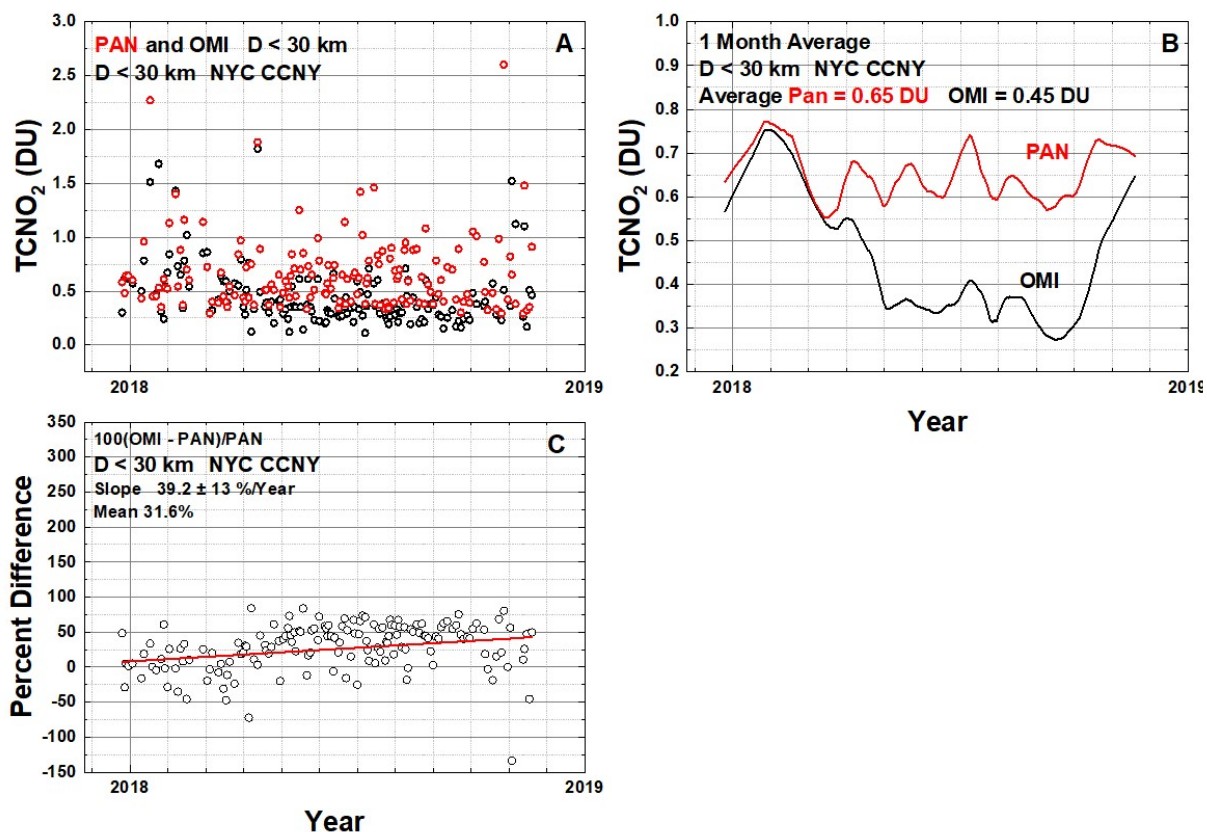
Fig. 10 TCNO$_2$ overpass time series for CCNY in Manhattan, New York City. OMI pixels are at a distance D < 30 km from CCNY. Panel A: OMI overpass TCNO$_2$ (Black) compare with OMI (Red). Panel B: Monthly Lowess(f) fit to the daily overpass data. Panel C: Percent difference 100(OMI – PAN)/PAN calculated from the data in Panel A

700

701 **Figure 10**
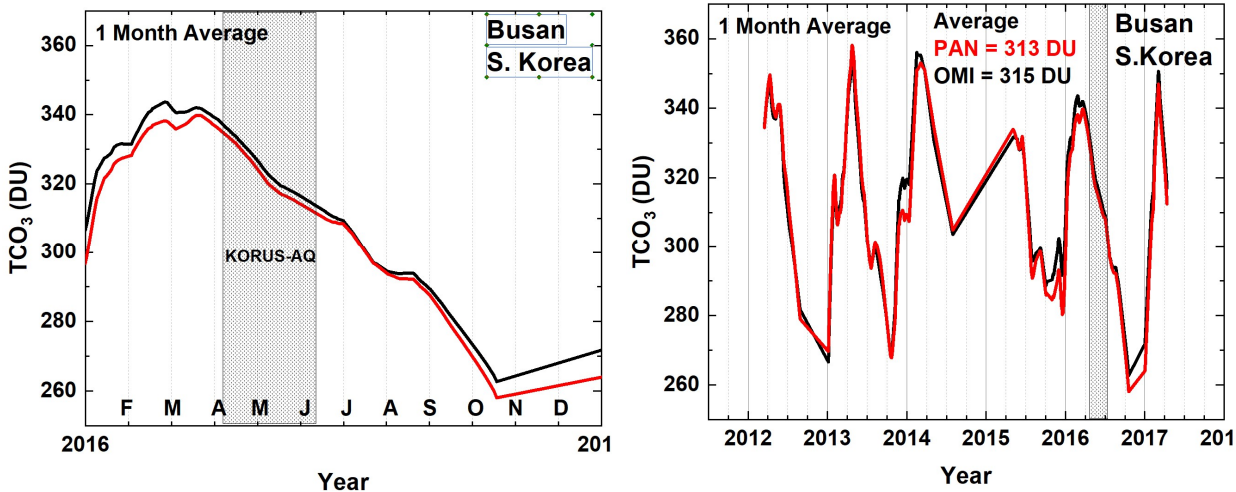
Fig. A1 Monthly average values of TCO₃ for OMI and PANDORA at OMI overpass times for Busan South Korea. Shaded area represents the KORUS-AQ campaign period.

702

703

704   **FIGURE A1**

705
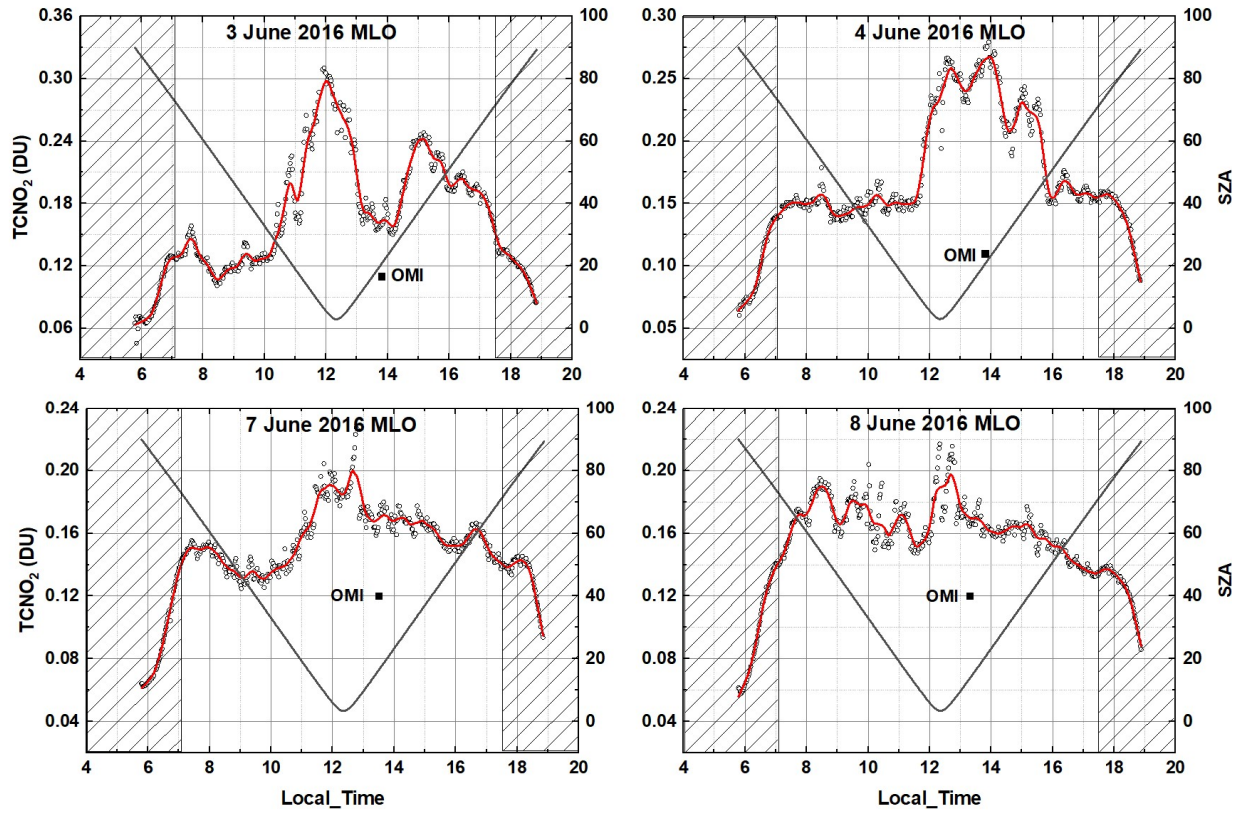
Fig. A2. The diurnal variation of $TCNO_2$ at MLO on 4 days during June 2016 compared to OMI $TCNO_2$ (small square). Shaded areas represent high SZA conditions where the PANDORA retrievals are not accurate.

706

707

708

709

710

711

712 **FIGURE A2**

713

714   **Author Contributions**: Jay Herman produced all of the figures and text, Jhoon and Jae Kim contributed

715   the Korean PANDORA data, Manvendra Dubey contributed the data from Waterflow, New Mexico and

716   the CO_2 analysis, Marcel Raponi contributed the Buenos Aires PANDORA data, And Maria Tzortziou

717   contributed the PANDORA data from CCNY.

718